○	Katayama S., Futaki S., et al	Acylation of octaarginine: Implication to the use of intracellular delivery vectors.	J Control Release	149	29-35	2011
○	Akita H., Futaki S., et al	Nanoparticles for ex vivo siRNA delivery to dendritic cells for cancer vaccines: Programmed endosomal escape and dissociation.	J Control Release	149	58-64	2011
○	Nakase I., Futaki S., et al	Efficient intracellular delivery of nucleic acid pharmaceuticals using cell-penetrating peptides.	Acc Chem Res	印刷中		2011
○	Tan H., Seno M., et al	The conformational polymorphism of the green fluorescent protein.	Molecular Biology	46(1)	142-148	2012
○	Hirose H., Futaki S., et al	Transient focal membrane deformation induced by arginine-rich peptides leads to their direct penetration into cells.	Mol Ther	印刷中		2012
○	Nakase I., Futaki S., et al	Accumulation of arginine-rich cell-penetrating peptides in tumors and the potential for anticancer drug delivery in vivo.	J Control Release	印刷中		2012

Ⅳ. 研究成果の刊行物・別刷

Biomaterials 30 (2009) 1746–1755

Contents lists available at ScienceDirect

Biomaterials

journal homepage: www.elsevier.com/locate/biomaterials

Delivery of sodium borocaptate to glioma cells using immunoliposome conjugated with anti-EGFR antibodies by ZZ-His

Bin Feng [a], Kazuhito Tomizawa [a,b,*], Hiroyuki Michiue [a], Shin-ichi Miyatake [c], Xiao-Jian Han [a], Atsushi Fujimura [a], Masaharu Seno [e], Mitsunori Kirihata [d], Hideki Matsui [a]

[a] Department of Physiology, Okayama University Graduate School of Medicine, Dentistry and Pharmaceutical Sciences, 2-5-1 Shikata-cho, Okayama 700-8558, Japan
[b] Department of Molecular Physiology, Faculty of Medical and Pharmaceutical Sciences, Kumamoto University, Kumamoto 860-8558, Japan
[c] Department of Neurosurgery, Osaka Medical College, 2-7 Daigaku-machi, Takatsuki Osaka 569-8686, Japan
[d] Department of Bioscience and Informatics, Graduate School of Life and Environmental Sciences, Osaka Prefecture University, 1-1 Gakuen-machi, Sakai 599-8531, Japan
[e] Department of Bioscience and Biotechnology, Faculty of Engineering, Okayama University Graduate School of Natural Science and Technology, Okayama 700-8530, Japan

ARTICLE INFO

Article history:
Received 1 October 2008
Accepted 4 December 2008
Available online 1 January 2009

Keywords:
Glioma cells
BNCT
EGFR
Immunoliposome
Drug delivery

ABSTRACT

Nanoparticles are effective of delivering cargo into cells. Here, sodium borocaptate (BSH) was encapsulated in liposomes composed of nickel lipid, and anti-epidermal growth factor receptor (EGFR) antibodies were conjugated to the liposomes using the antibody affinity motif of protein A (ZZ) as an adaptor (immunoliposomes). The immunoliposomes were used to deliver BSH into EGFR-overexpressing glioma cells. Immunohistochemical analysis using an anti-BSH monoclonal antibody revealed that BSH was delivered effectively into the cells but not into EGFR-deficient glioma or primary astrocytes. In an animal model of brain tumors, both the liposomes and the BSH were only observed in the tumor. Moreover, the efficiency of ^{10}B's delivery into glioma cells was confirmed by inductively coupled plasma-atomic emission spectrometry (ICP-AES) both *in vitro* and *in vivo*. The results suggest that this system utilizing immunoliposomes provides an effective means of delivering ^{10}B into glioma cells in boron neutron capture therapy (BNCT).

1. Introduction

Glioblastoma multiforme (GBM) is one of the most malignant and aggressive brain tumors. Although at present, treatment mainly consists of surgery and radiotherapy [1], it is difficult to remove all tumor tissues without severe damage to the brain, and healthy brain tissue is less tolerant of conventional radiotherapy than tumor tissue.

Boron neutron capture therapy (BNCT) provides a way to selectively destroy malignant cells and spare normal cells. BNCT is a binary method for the treatment of cancer based on the tumor-selective delivery of ^{10}B followed by radiation with low energy thermal neutrons [2]. It is assumed that the selective accumulation of ^{10}B in tumors will cause the killing of cancer cells and induce a therapeutic effect [3]. BNCT has been applied clinically for the treatment of malignant brain tumors, malignant melanoma, head and neck cancer, and hepatoma [4]. For effective BNCT, enough ^{10}B must be encapsulated in the tumor and a high ratio of tumor to blood is needed. Different approaches have been proposed for delivering ^{10}B into tumor cells, including the use of boronated macromolecules such as monoclonal antibodies and microparticles such as liposomes, etc. [2]. However, these methods have several disadvantages, such as low delivery efficiency, a lack of specificity and stability *in vivo*, and the high cost of preparing nanoparticles. Two boron compounds, sodium borocaptate (BSH) and boronophenylalanine (BPA), are undergoing clinical trials [5]. BPA is an analog of an essential amino acid and actively carried to brain tumors. However, it also accumulates in normal brain tissue. By contrast, BSH accumulates little in normal tissue but accumulates insufficiently in tumors compared with BPA [6]. Therefore, an easy-to-prepare and universal ^{10}B delivery system is still awaited.

In recent years, drug delivery research has increasingly focused on antibody-targeting liposomes in the treatment of cancers including glioblastoma [7]. Liposomes are unilamellar phospholipid vesicles with high interior encapsulation for water-soluble compounds such as borane ions [8]. Targeted liposomes provide an advantage over untargeted liposomes not because of increased localization to tumor sites but because of increased interaction with

* Corresponding author. Department of Molecular Physiology, Faculty of Medical and Pharmaceutical Sciences, Kumamoto University, Kumamoto 860-8558, Japan. Tel.: +81 96 373 5050; fax: +81 96 373 5052.
E-mail address: tomikt@kumamoto-u.ac.jp (K. Tomizawa).

0142-9612/$ – see front matter © 2008 Elsevier Ltd. All rights reserved.
doi:10.1016/j.biomaterials.2008.12.010

the target cell population once localized to the tumor sites [9]. For targeted ^{10}B delivery in BNCT, immunoliposomes have been employed by linking tumor-targeting ligands to liposome such as antibodies or receptor ligands such as folate [10], transferrin [11] and epidermal growth factor (EGF) [12].

EGFR is a 170-kDa transmembrane tyrosine kinase and the *EGFR* gene is often amplified in human GBMs. EGFRvIII, which has an in-frame deletion of exons 2–7 of the extracellular domain of the *EGFR* gene, is constitutively expressed and amplified in up to 57% of GMBs [13,14]. EGFR is overexpressed in GMB, but is undetectable or weakly expressed in normal brain. Therefore, EGFR is an attractive molecular target for the specific delivery of therapeutic agents to high-grade gliomas [15,16]. An antibody can be directly linked to a liposome through covalent conjugation to a functional group on the liposome [17] or can be post-inserted into a preformed liposome via the micelles of an antibody–lipid conjugate [18,19].

We previously used hollow bionanocapsules (BNCs) composed of modified L protein (the hepatitis B virus surface antigen) for targeting brain tumors [20]. In the present study, BSH was encapsulated into a nickel-liposome and recombinant ZZ-His (IgG Fc-binding motif) was used as an adaptor to conjugate anti-EGFR antibody to the nickel-liposome, resulting in an immunoliposome. Three glioma cell lines, parental U87 glioma cells (PAU87) and human wild-type *EGFR* and *EGFRvIII*-transfected U87 glioma cells (U87 WT and U87 ΔEGFR), were used to evaluate the efficiency with which ^{10}B was delivered by the immunoliposomes *in vitro* and *in vivo*.

2. Materials and methods

2.1. Lipids and chemicals

1,2-Dioleoyl-*sn*-glycero-3-[(*N*-(5-amino-1-carboxypentyl)iminodiacetic acid)-succinyl] nickel (abbreviated as DOGS-NTA-Ni) and the fluorescent analog 25-[*N*-[(7-nitrobenz-2-oxa-1,3-diazol-4-yl)-methyl]amino]-27-norcholesterol (abbreviated as NBD-cholesterol) were purchased from Avanti Polar Lipids (Alabastar, AL). DOPC, DOPG and DSPE-PEG_{2000} were obtained from Nippon Oil and Fats (Tokyo, Japan). BSH ($Na_2B_{12}H_{11}SH$, ^{10}B enriched > 99%) was purchased from Katchem Ltd. (Czechoslovakia). Chloroform, diethyl ether and cholesterol were acquired from Wako Pure Chemicals (Japan).

2.2. Preparation of liposomes

Liposomes composed of DOPC:DOPG:DOGS-NTA-Ni:CH:DSPE-PEG_{2000} (3:3:1:4:0.1, molar ratio) were prepared according to the reverse-phase evaporation (REV) method [11] with slight modification. Briefly, 100 μmol of lipid was dissolved in 2 mL of a chloroform/diethyl ether mixture (1:1 v/v), and 1 mL of a 50 mM BSH solution was added. The ratio of the organic to aqueous phase was 2:1. To prepare liposomes for experiments *in vivo*, a 300 mM BSH solution was used. The mixture was sonicated for 1 min to form a W/O emulsion and evaporated with reduced pressure in a rotary evaporator at 50 °C until a gel was formed. Ten cycles of freezing (dry ice) and thawing (60 °C water bath) were then applied. To obtain liposomes with a homogeneous size distribution, the liposome emulsion was extruded through a polycarbonate membrane 100 nm in pore size using an extruder device at 60 °C. The mean diameter and zeta-potential of the prepared liposomes were determined with an electrophoretic light scattering spectrophotometer (ELS-8000, Photal, Tokyo, Japan). Unencapsulated free BSH was removed by an Amersham sephadex G-50 column (1 × 30 cm). For the preparation of fluorescent liposomes, 1 mol% of NBD-cholesterol was added to the lipid solution.

2.3. Expression and purification of ZZ-His protein

The *ZZ* gene was cloned into pET-22b (+) (Novagen, Madison, WI) and introduced into *E. coli* BL21 (DE3). The expression and purification of ZZ-His were performed as described [21]. Briefly, recombinant proteins were induced by the addition of 1 mM isopropyl-β-D-thiogalatopyranoside (IPTG) when the optical density (OD) of the cell culture at 600 nm reached 0.6. The expressed proteins were purified from the supernatant using ProBond Nickel-chelating resin (Invitrogen) and dialysed against PBS (pH 7.4) at 4 °C for 24 h. The proteins were stored at −80 °C prior to use.

2.4. Cell lines and cell culture

Three human glioma cell lines (kindly donated by Professor Webster K. Cavenee of the University of California at San Diego) were used. U87 ΔEGFR expresses EGFRvIII (145 kDa); U87 WT expresses wild-type EGFR (170 kDa); and PAU87 (parental) expresses no EGFR. The cells were maintained in Dulbecco's modified Eagle's medium (DMEM) (GIBCO) with 10% fetal bovine serum (FBS), penicillin and streptomycin at 37 °C in a humidified atmosphere containing 5% CO_2. Rat primary astrocytes were prepared from a newborn Wistar rat (Japan SLC, Inc.) as described previously [22].

2.5. Antibody-mediated ZZ delivery to EGFR-overexpressing glioma cells

To identify the ability of antibody-directed ZZ-His delivery, we first analyzed the expression level of EGFR in different cells. PAU87, U87 ΔEGFR, and U87 WT cells and primary astrocytes were homogenized by sonication in a boiling buffer containing 1% SDS and Western blotting was carried out as described previously [23]. The blots were probed with an anti-EGFR mouse mAb (101-7300-0, Katayama Chemical Inc., Japan) or the anti-EGFR rat mAb ICR10 (Abcam, Cambridge, UK). After incubation with the appropriate secondary antibody conjugated with horseradish peroxidase (Sigma–Aldrich), positive bands were visualized using an enhanced chemiluminescence detection system (Amersham Biosciences, Pittsburgh, PA).

For delivering ZZ-His into cells via antibody, 18 μg of ZZ-His and anti-EGFR mouse antibody were mixed at a molar ratio of 5 to 1 (ZZ-His to antibody) in 200 μL of PBS (pH 7.4) and rotated at 4 °C for 2 h. Then the ZZ-mAb complex was added to PAU87, U87 ΔEGFR, U87 WT and the primary astrocytes. As a control, only ZZ-His was added. After 2 h of incubation, the cells were washed with PBS twice and treated with 0.025% trypsin to remove surface-binding antibody. They were then resuspended in PBS twice before sonication and subjected to Western blotting using an anti-His (C-term) mouse monoclonal antibody (Invitrogen).

2.6. Analysis of liposome–ZZ–mAb complex (immunoliposome) by ultracentrifugation, Western blotting and lipid measurements

To determine the binding ability of nickel-liposomes and ZZ-His, the two were mixed at a molar ratio of 20–1 (nickel lipid: ZZ-His), rotated at room temperature for 1 h, and then subjected to sucrose gradient ultracentrifugation. Two milliliters of each 10, 20, 30, 40 and 50% sucrose solution was used to prepare the gradient. After 16 h of ultracentrifugation at 35,000 rpm using a Beckman coulter optima-LE-80k ultracentrifuge (rotor SW 41), 1 mL was drawn out and samples were resolved by SDS-PAGE and then transferred to nitrocellulose membranes (Hybond ECL, Amersham Biosciences). Western blotting was performed as described above. The lipid in each fraction was analyzed by the DAOS method using a Phospholipids C reagent kit (Wako Pure Chemical Inc. Ltd., Japan).

For a large amount of immunoliposome, the free ZZ protein was separated by a Sepharose CL-4B column (15 × 70 mm) and the collected liposome–ZZ was concentrated with Amicon Ultra-15 centrifugal filter devices (Millipore). The antibody was conjugated to the liposome–ZZ at a molar ratio of 1 to 20 (mAb:ZZ) and the free antibody was separated with a Sepharose CL-4B column.

2.7. Immunohistochemical analysis (IHC) and measurement of ^{10}B content in vitro

Immunoliposomes were prepared with anti-EGFR rat or mouse mAb for IHC and measuring ^{10}B content, respectively. IHC was carried out to analyze the distribution of ^{10}B *in vitro*. Cells were incubated for 24 h and BSH, liposome, liposome–ZZ, and immunoliposome were added. The final ^{10}B concentration was 1 μg/mL and the antibody concentration was 3 μg/mL. After 3 h of incubation, the cells were washed with PBS twice, fixed with 4% paraformaldehyde (PFA) for 10 min, and then incubated with anti-BSH mouse mAb [24]. The secondary antibody was Cy3-conjugated mouse IgG. Fluorescence signals were observed using a confocal laser microscope (FluoView, Olympus, Japan).

To detect ^{10}B in cells, BSH, liposome, liposome–ZZ, and liposome–ZZ–mAb were added in 6-cm dishes. After 3 h of incubation, the cells were washed with PBS, dissolved in 200 μL of concentrated nitric acid overnight, and diluted with 5 mL of MillQ water. For liposome–ZZ and immunoliposome-treated cells, 250 mM of imidazole was used for an additional wash to remove surface-bound liposome. The ^{10}B content was measured by inductively coupled plasma-atomic emission spectrometry (ICP-AES, Vista Pro, Seiko Instruments, Japan).

To analyze the effect of the antibody concentration on the delivery of ^{10}B, 1 mM of liposome was incubated with U87 ΔEGFR cells in the presence of 0.1, 0.5, 1, 3, 5, 10, or 50 μg/mL of mAb for 3 h. To analyze the effect of time on the delivery, 3 μg/mL of antibody was used and U87 ΔEGFR cells were incubated with 1 mM of immunoliposome for 1, 3, 5, 7, 12 and 24 h. The ^{10}B measurements were carried out as described above.

2.8. Brain tumor model and detection of immunoliposomes in vivo

U87 ΔEGFR cells (5×10^5 cells/5 μL) were injected into the striatum of female 4- to-6 week-old nude mice (15-20 g, BALB/c Slc-nu/nu; Japan SLC) as described [24]. After two weeks, 400 μL of NBD-liposome and NBD-immunoliposome was administered into tumor-bearing mice intravenously via the tail. After 4 h and 24 h, the mice were sacrificed and the brains were placed in PBS. Sections of 10-μm thickness were cut on a microtome (CM 1850, Leica Microsystems, Wetzlar, Germany). IHC was

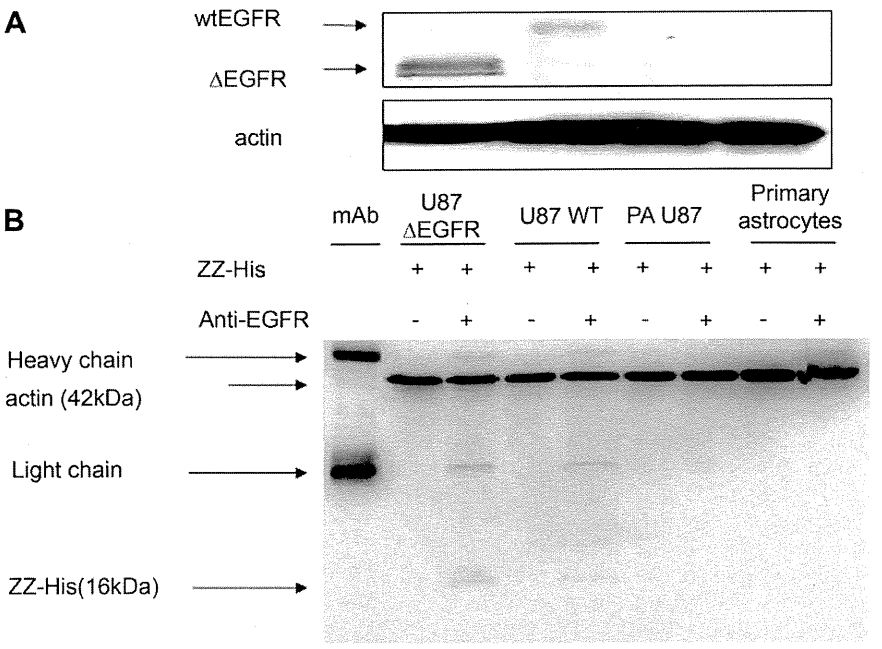

Fig. 1. EGFR expression level in different cell lines and antibody-mediated ZZ-His delivery. (A) Cell lysates of primary astrocytes and glioma cell lines U87 ΔEGFR, U87 WT, and PAU87 were subjected to 6% SDS-PAGE and transferred to PVDF membranes. Anti-EGFR mouse monoclonal antibody was used for detection of the wild-type and vIII EGFR. (B) ZZ-mAb and ZZ were incubated with cells for 2 h and the delivered proteins were detected by anti-His mouse mAb.

carried out as described above. The fluorescence labeling of liposomes was observed immediately after the sections were prepared.

For the analysis of the distribution of ^{10}B, immunoliposomes and liposomes were injected via the tail at a dose of 35 mg ^{10}B/kg. Tumor, normal brain, liver, and blood were sampled at 4, 12, 24, and 48 h post-administration, and the samples were digested with a nitric acid solution overnight and diluted with MillQ water for ICP-AES.

2.9. Statistical analysis

Data are shown as the mean ± S.E. Data were analyzed using Student's *t*-test to compare the two conditions, and $p < 0.05$ was considered significant.

3. Results

3.1. Antibody-mediated delivery of ZZ into glioma cells

EGFR levels in each cell line were determined by Western blotting using an anti-EGFR monoclonal antibody (mAb). The mAb detected EGFR in ΔEGFR-expressing U87 cells (U87 ΔEGFR) and wild-type EGFR-expressing cells (U87 WT) (Fig. 1A). In contrast, EGFR expression was undetectable in PAU87 cells and primary astrocytes. Thereafter, we examined the ability of the mAb to target EGFR-overexpressing glioma cells. The Western blotting showed that the mAb and ZZ-His were detected in U87 ΔEGFR and U87 WT cells when ZZ was bound with the antibody (Fig. 1B). In contrast, neither mAb nor ZZ-His was detected without conjugation with the anti-EGFR mAb (Fig. 1B). Moreover, no antibody or ZZ was detected in PAU87 cells and primary astrocytes (Fig. 1B). These results suggest that the anti-EGFR mAb is capable of targeting glioma cells expressing wild-type and vIII EGFR.

3.2. Identification of liposome–ZZ–mAb complex

When 10 mol% of DOGS-NTA-Ni and 1 mol% of DSPE-PEG_{2000} were used in the liposome formulation, no aggregation occurred. It was reported that NTA-Ni increased the sensitivity and DSPE-PEG_{2000} reduced the aggregation [25]. Therefore, to identify the ability of ZZ-His to bind with mAb and nickel-liposomes containing 10 mol% DOGS-NTA-Ni and 1 mol% DSPE-PEG_{2000}, we carried out ultracentrifugation and Western blot analyses. The ultracentrifugation indicated that the nickel-liposomes bound with ZZ-His effectively. The positions in different layers are shown in Fig. 2A. When 1 mol% DSPE-PEG_{2000} was used in the liposome, the distribution was the same as that without DSPE-PEG_{2000} (data not shown). As shown in Fig. 2B, most of the PEG-liposomes were in the first layer after ultracentrifugation. When ZZ-His was mixed with the nickel-liposome and mAb, the liposomes occurred in the fourth and fifth layers. Results of Western blotting in Figs. 2C–F show that the ZZ, liposome, and antibody are all in the same layer (fractions 4 and 5), while free ZZ-His and mAb are in the first and third fractions, respectively. These results suggest that mAb is effectively bound to liposome via ZZ adaptor. When the molar ratio of nickel lipid to ZZ was 20:1, about half of the ZZ bound with liposomes (Fig. 2D). The ratio was adjusted to 40:1 in the subsequent experiment.

The Western blotting and lipid analysis also indicated that the binding of the nickel-liposome to ZZ and of ZZ to the mAb was specific because the liposome showed no ability to bind ZZ when nickel lipid was not used (data not shown). When ZZ was not used, the nickel-liposome showed no binding with mAb (data not shown). A scheme of the immunoliposome is shown in Fig. 3A. The diameter of the liposome is about 100 nm, but when ZZ and mAb are added, the diameter of the immunoliposome increases to 130 nm (Fig. 3B). The *z*-potential also increases, from −44.74 to −24.67 mV (Fig. 3C). The immunoliposomes were used for *in vivo* experiments.

3.3. Delivery of BSH into glioma cells in vitro

We examined the effect of the immunoliposomes on the delivery of ^{10}B in different cell lines. The cells were incubated with the immunoliposomes for 3 h and the delivery of ^{10}B was then investigated with IHC using the anti-BSH mAb (Fig. 4). BSH was not

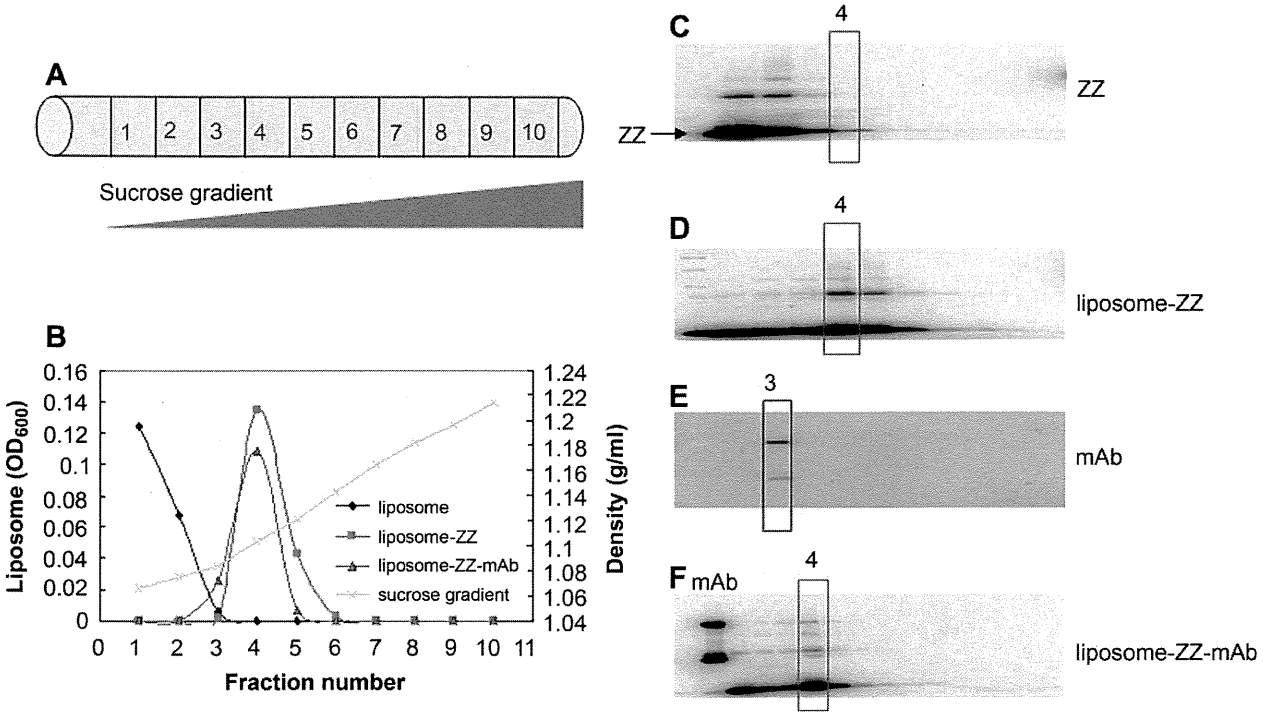

Fig. 2. Analysis of the liposome–ZZ–mAb complex. (A) Distribution of each fraction in a sucrose gradient. (B) Phospholipids in different fractions were measured by the DAOS method after ultracentrifugation and absorbance at OD_{600} was used to indicate the position of liposomes. (C, D) The position of ZZ was identified by anti-His antibody after ultracentrifugation in ZZ and liposome-ZZ samples. (E, F) The positions of mAb and ZZ were identified by anti-His antibody after ultracentrifugation in mAb and liposome–ZZ–mAb samples.

detected in primary astrocytes and only a small amount of BSH was delivered into PAU87 cells (Fig. 4). The results of ICP-AES were consistent with those of IHC (data not shown). In contrast, BSH was delivered in almost all U87 ΔEGFR and U87 WT cells expressing vIII EGFR and wild-type EGFR, respectively (Fig. 4). To demonstrate that BSH was actually present inside glioma cells and to exclude the possibility that it was just attached to the surface of the cells, serial optical sections of 2 μm taken along the *Z*-dimension of the immunostained cells were collected with a confocal microscope (Supplementary material). Signal for BSH on the surface of the cells was weak and most BSH was observed in the cells (Supplementary material). Moreover, strong signals were observed in the nucleus. To further investigate whether BSH delivered by immunoliposomes functions as ^{10}B in glioma cells, ICP-AES was performed (Fig. 5A). In U87 ΔEGFR and U87 WT cells incubated with control liposomes without the anti-EGFR antibody, the ^{10}B level was low. In contrast, a high level of ^{10}B was detected in the cells incubated with immunoliposomes (Fig. 5A). Moreover, immunoliposomes did not deliver ^{10}B into PAU87 cells (Fig. 5A). These results suggest that immunoliposomes conjugated with anti-EGFR antibodies efficiently deliver ^{10}B in glioma cells expressing EGFR.

3.4. Effect of antibody concentration and time course on BSH delivery

We examined the dose-dependent effect of the antibody on the efficiency of ^{10}B delivery. Following 3 h of incubation with immunoliposomes in the presence of 0.1, 0.5, 1, 3, 5, 10, or 50 μg/mL of anti-EGFR antibody, the cells were washed twice with PBS containing Ni-chelating components (250 mM imidazole) to remove surface-bound liposomes. ICP-AES revealed that 0.5 μg/mL of antibody was effective for the delivery of ^{10}B compared with liposomes without the antibody (Fig. 5B). In the time-course experiment, 3 μg/mL of antibody was used for the detection of ^{10}B and cells were incubated with immunoliposomes for 1, 3, 5, 7, 12 and 24 h. The ^{10}B content of cells increased with time (Fig. 5C). When cells were incubated with immunoliposomes at 4 °C, little ^{10}B was detected inside them (data not shown), suggesting that the uptake of immunoliposomes was temperature-dependent and the immunoliposomes were internalized into cells by endocytosis.

3.5. In vivo delivery of BSH in brain tumor by immunoliposomes

To observe the distribution of the liposome and BSH *in vivo*, we injected NBD-liposomes and NBD-immunoliposomes into the tail of nude mice two weeks at the tumor engraftment. In freshly prepared brain slices, fluorescence could be seen in the tumor and blood vessel wall 4 h after the injection (Figs. 6A and D). In normal tissues, strong fluorescence was seen only in the blood vessel wall (arrowheads in Fig. 6E). In the NBD-liposome-injected mice, no fluorescence was seen in the tumor (Fig. 6G). Signal's distribution indicates that the immunoliposomes were delivered into the tumor via the blood stream, and the delivery was antibody-dependent. BSH's distribution was examined by IHC using the anti-BSH mAb. BSH was clearly detected in the tumor whereas it was undetectable in normal tissue (Figs. 7A and B). A low level of BSH was observed in both tumor and normal tissues of the mice treated with the control liposome without conjugation of the anti-EGFR mAb (Figs. 7D and E). In immunoliposome-treated mice for 24 h, BSH was detected in the tumor and surrounding regions (Fig.7G and H).

We finally compared ^{10}B content among each tissue in this model of brain tumors. Immunoliposomes effectively delivered BSH to tumors compared with liposomes (Fig. 8). In immunoliposome-treated mice, the amount of ^{10}B in the tumor reached

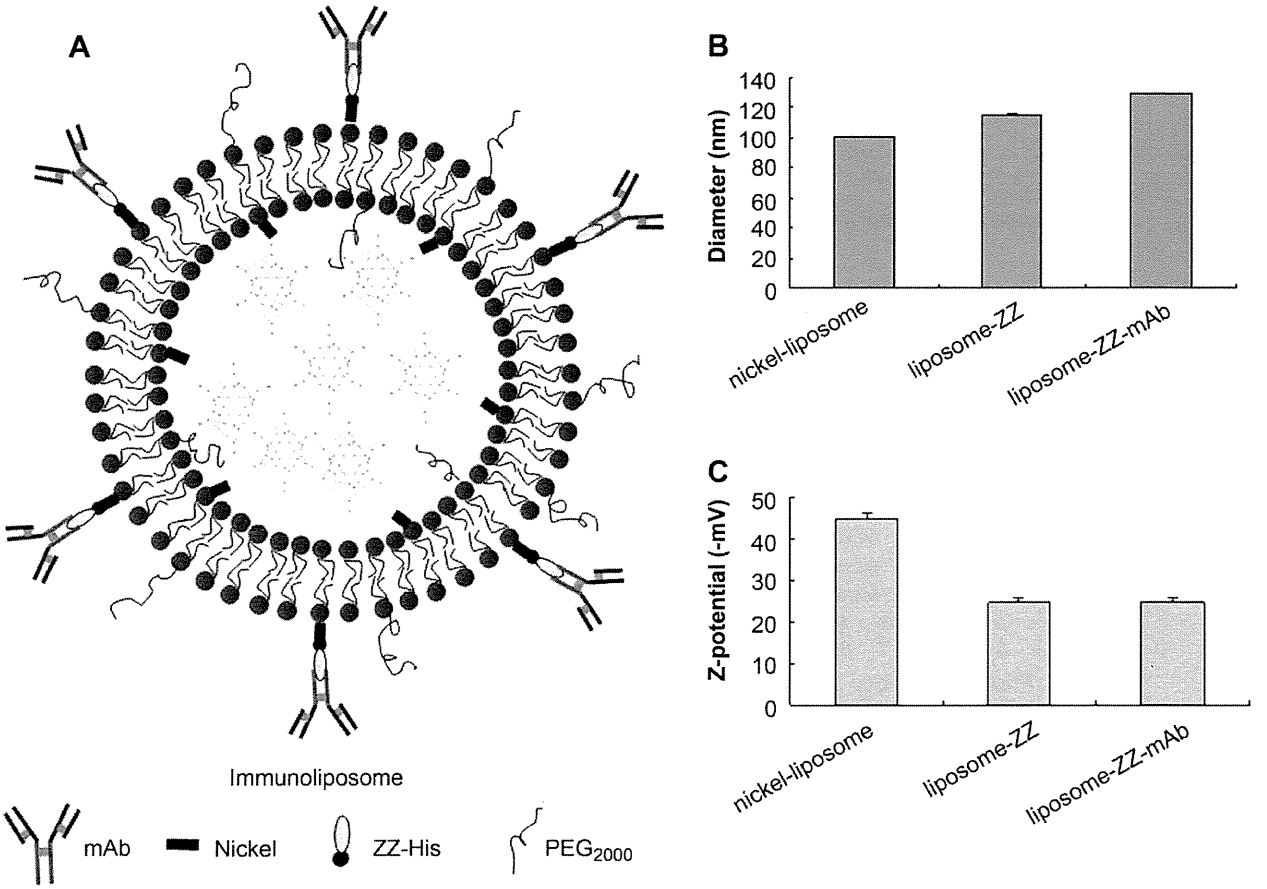

Fig. 3. Characteristics of the immunoliposomes. (A) Scheme of components of the immunoliposome. (B, C) Diameter and z-potential of the nickel-liposome, liposome–ZZ and immunoliposome.

28.36 ± 7.63 μg/g 24 h after the injection and remained high until the 48 h mark (21.38 ± 5.31 μg/g). In liposome-treated samples, on the other hand, the ^{10}B content of tumors at 24 and 48 h was 3.45 and 2.97 μg/g, respectively (Fig. 8A). In normal brain tissue of the mice treated with immunoliposomes and liposomes, ^{10}B content was low at all time points (Fig. 8B). In liver, ^{10}B levels peaked 12 h after the injection and then decreased in a time-dependent manner (Fig. 8C). In blood, ^{10}B levels reached a maximum 4 h after the injection of immunoliposomes and rapidly decreased 12 h after the injection (Fig. 8D).

4. Discussion

The aim of the present study was to develop a novel ^{10}B delivery system for targeting glioma cells. Since the appearance of BNCT in the 1950s, different methods of delivering ^{10}B into tumor cells have been investigated [2,4], though only BSH and BPA have been used clinically. BSH is thought to penetrate tumor tissue through a disrupted blood–brain barrier (BBB) and thus accumulates little in normal brain tissue [26]. BPA is an analog of an essential amino acid (tyrosine) and is actively taken up by tumor cells but also accumulates measurably in normal brain [5]. The specific accumulation of ^{10}B in tumor tissue is still a limitation to the use of this technology. In the present study, we encapsulated BSH in liposomes and used a universal adaptor (ZZ) to conjugate an anti-EGFR mAb to target glioma cells.

The wild-type EGFR and its isoforms (variant III) are considered prime targets for the specific delivery of a variety of diagnostic and therapeutic agents [9,27,28]. In BNCT, mAb or EGF-conjugated immunoliposomes and boronated mAb have been used to deliver ^{10}B into glioma cells [7,12,14,29]. The anti-EGFR antibody used in this study recognized both wild-type and vIII EGFR, so ZZ-His bound with the mAb could be effectively delivered into EGFR-overexpressing glioma cells. In our ^{10}B delivery system, the ability of ZZ to bind the nickel-liposome was not affected by the addition of 1% DSPE-PEG_{2000} and the liposome–ZZ complex showed the same position as the naked nickel-liposome–ZZ after ultracentrifugation (data not shown). Chikh et al. [30] reported that the addition of 5 mol% of DSPE-PEG_{2000} caused a slight change in the rate of binding, but the incorporation efficiency of His-tagged peptide did not change. The binding of DOGS-NTA-Ni with ZZ-His is not achieved at a theoretical ratio. When a molar ratio of 20:1 (DOGS-NTA-Ni:ZZ-His) was used, only about half the amount of ZZ could be conjugated with the liposome, and the liposome–ZZ complex was in the fourth layer (Fig. 2D). When the ratio was adjusted to 40:1, no free ZZ was detected by Western blotting after ultracentrifugation (data not shown). The interaction of DOGS-NTA-Ni with His-tags has been reported to be stronger than or equivalent to that of antibody interactions (10^{-6} to 10^{-9} M), with a dissociation constant (k_d) in the range of 10^{-6} to 10^{-13} M at pH 7–8 depending on the protein and location of the His-tag on the protein [31,32]. When the molar ratio of ZZ to mAb was 25:1, all the liposome–ZZ–mAb complexes occurred in the four and fifth layers after ultracentrifugation. For the preparation of immunoliposomes, removal of free ZZ and mAb from the liposome–ZZ complex may be important, because free mAb or ZZ–mAb will bind to EGFR-overexpressing cells.

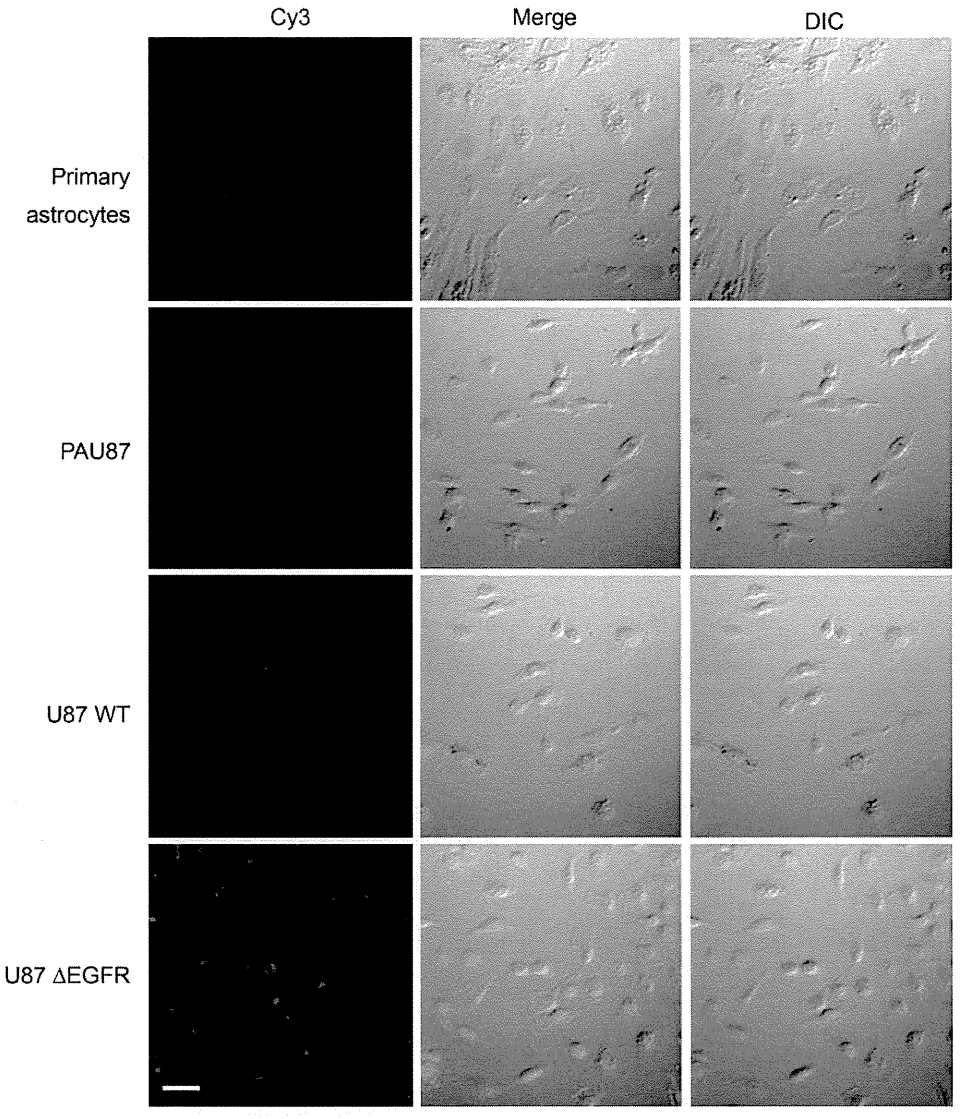

Fig. 4. Analysis by immunohistochemistry (IHC) of ^{10}B delivery by immunoliposomes in different cell lines. Immunoliposomes (liposome: 1 mM; anti-EGFR rat mAb: 3 μg/mL; ^{10}B: 1 μg/mL) were incubated with primary astrocytes, PAU87, U87 WT and U87 ΔEGFR for 3 h and fixed with 4% PFA. Anti-BSH mouse mAb was used as the primary antibody and Cy3-conjugated mouse IgG was used as the secondary antibody. The fluorescence signals were visualized using a confocal laser microscope. Bar = 50 μm.

The conjugation of ZZ-His protein at the surface of a liposome by DOGS-NTA-Ni will make the liposome more stable in blood. Moreover, the combination of ZZ and PEG inhibits interaction of the liposome and cells to some degree, and so inhibits non-specific endocytosis. Recently, NTA-Ni has been reported to attach His-tag peptides and proteins to the liposome [30]. van Broekhoven et al. [33] used NTA-Ni for surface mobilization of His-tagged antibodies for DC-specific receptor to DCs.

An advantage of using ZZ to bind with Fc of IgG is that complete-IgG-labeled liposomes may have shorter circulation times, due to the rapid identification and uptake of the Fc fragment by macrophages in circulation [34]. Allen et al. [35] reported that increasing the density of liposome-grafted antibodies resulted in a faster clearance of immnoliposomes from the circulation. To overcome this, an antibody fragment (Fab′ and scFV) that lacks the Fc portion was used, and showed identical circulation times with PEGylated non-immunolabeled liposome when conjugated to the free termini of PEGylated lipid [27].

Protein A has been widely used for purifying IgG because of its specific binding to the Fc domain of IgG through bioaffinity [36]. In this study, we used the ZZ motif (Fc-binding domain) as an adaptor to conjugate an antibody to the liposome, resulting in an immunoliposome. In this ^{10}B delivery system, the specificity and totality of the antibody are retained, and not affected by thiolation of the antibody during liposome's preparation. The His-tag at the C-terminus of ZZ is used not only for purification, but also for interaction with chelated divalent metal ions, nickel in the NTA-Ni lipid [37]. NTA forms a strong complex with four of the metal sites, leaving two additional sites for interaction with the His-tag present on the protein. After incubation in medium for 12 h, the immunoliposomes still deliver ^{10}B efficiently (data not shown), indicating the stability of liposome–ZZ–mAb in serum. Long-term stability of the immunoliposomes in serum will permit high levels of ^{10}B to accumulate in tumor cells *in vivo*.

Gliomas have a poor prognosis due to their exceptional ability to infiltrate normal brain tissue, often along blood vessels or nerve

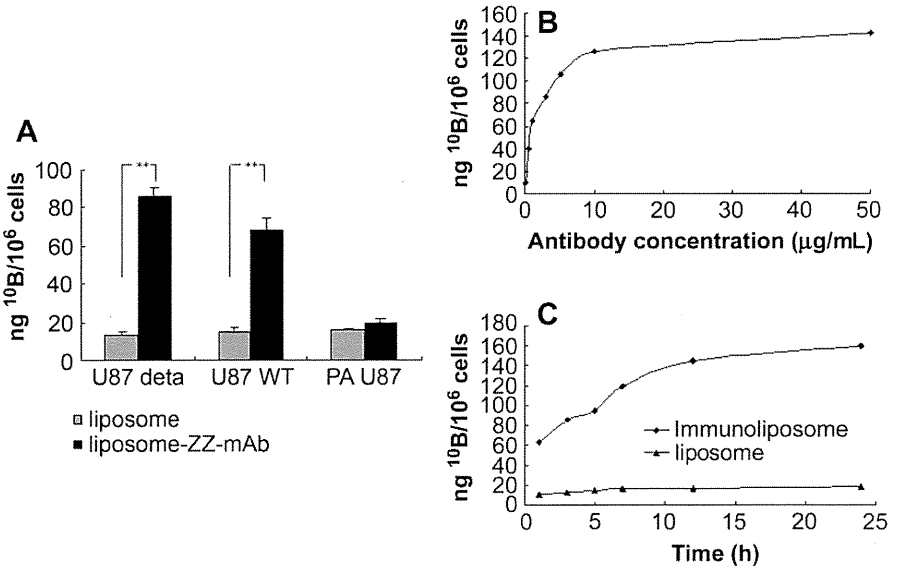

Fig. 5. ICP-AES of ^{10}B delivery by immunoliposomes *in vitro*. (A) After 3 h of incubation in medium containing 1 mM of liposomes or immunoliposomes (1 μg/mL of ^{10}B and 3 μg/mL of anti-EGFR mouse mAb) in a 6-cm dish, cells were treated with 0.025% trypsin and washed with 250 mM of imizadole and PBS, and amounts of internalized ^{10}B were detected. $n = 4$; ** $p < 0.01$. (B) Effect of antibody concentration on ^{10}B delivery. U87 ΔEGFR cells were incubated with 1 mM of immunoliposomes for 3 h in the presence of 0.1, 0.5, 1, 3, 5, 10, or 50 μg/mL of mAb and ^{10}B was detected. (C) Time course of ^{10}B delivery by immunoliposomes. Immunoliposomes and liposomes were incubated with U87 ΔEGFR cells for 1, 3, 5, 7, 12 and 24 h. At the indicated time, ^{10}B was measured.

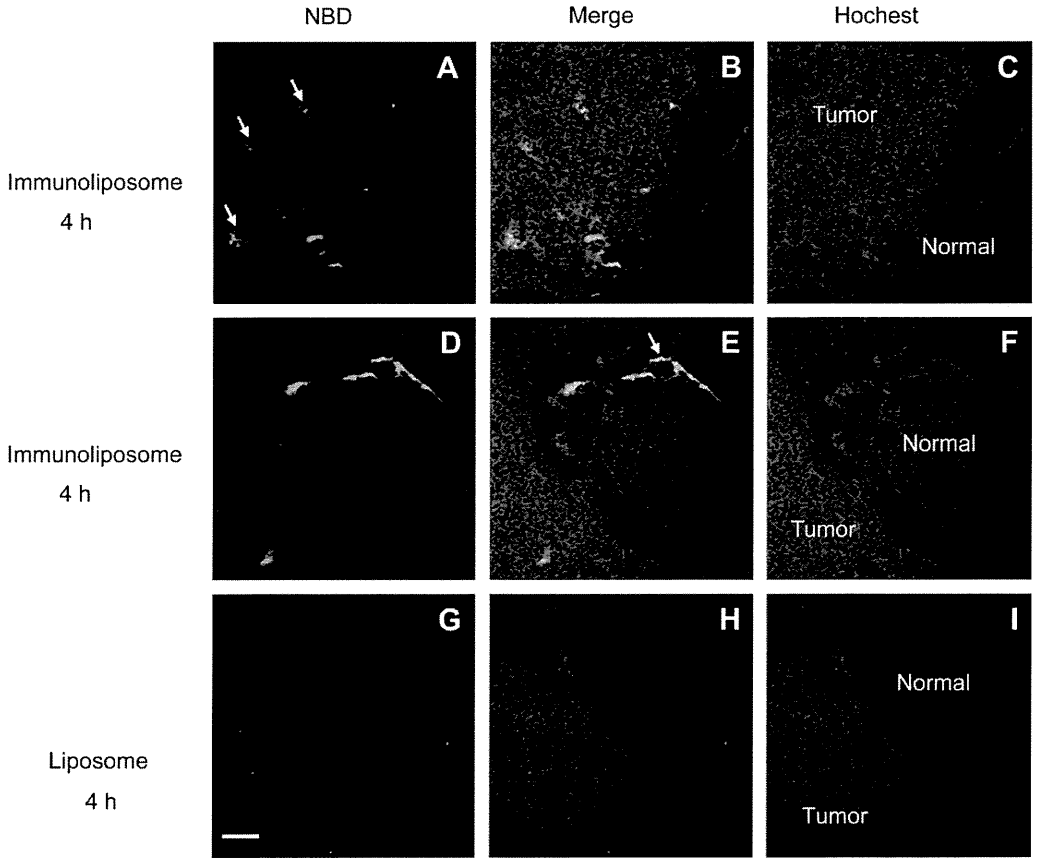

Fig. 6. Distribution *in vivo* of NBD-immunoliposomes. Four hundred microliters (liposome concentration: 50 mM; antibody concentration: 180 μg/mL) of NBD-immunoliposome or NBD-liposome was injected via the tail into nude mice two weeks after tumor engraftment. Green fluorescence of NBD and blue fluorescence of hochest were used to indicate the positions of the liposomes and tumor 4 h after injection, respectively. (A,D,G) NBD-fluorescence images (10×) of freshly prepared brain slices. (C,F,I) Hochest-fluorescence images (10×) of freshly prepared brain slices. (B,E,H) Merging of the NBD and hochest signals. Arrows indicate the positions of blood vessels. Bar = 200 μm.

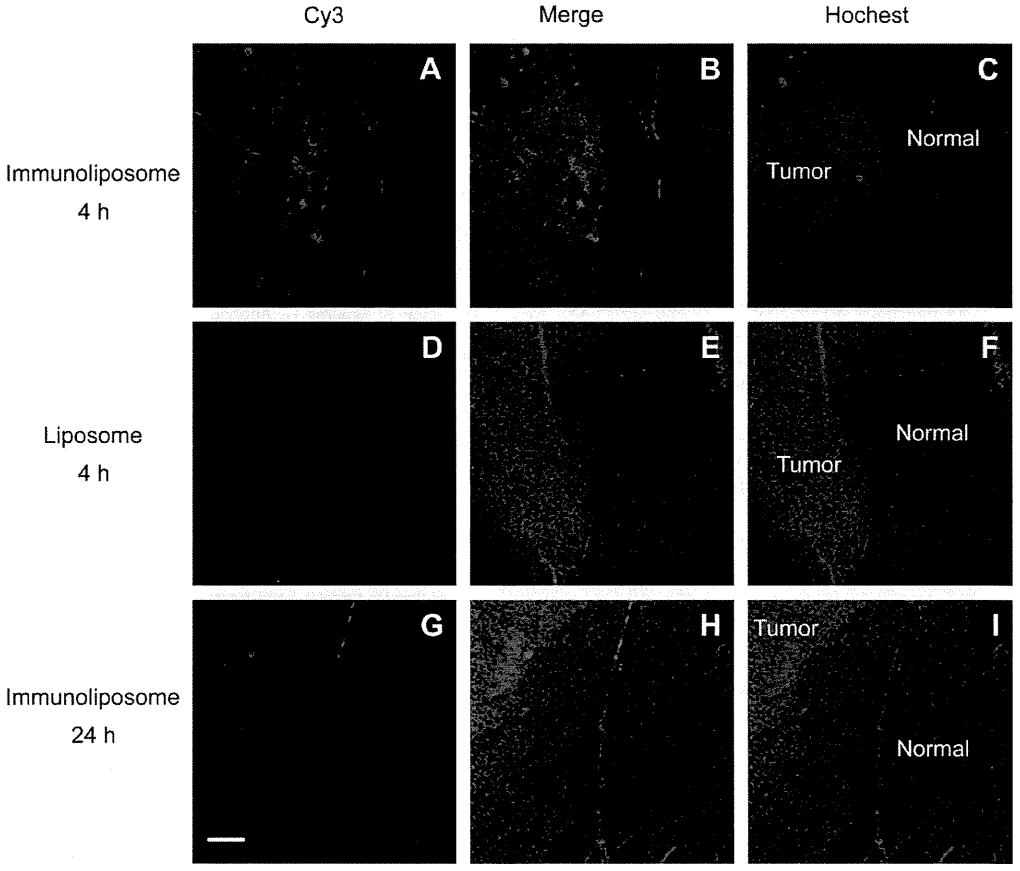

Fig. 7. IHC analysis of BSH's distribution *in vivo*. Four hundred microliters of immunoliposomes or liposomes was injected into the tail of nude mice two weeks after tumor engraftment. Slices were prepared 4 and 24 h post-injection. Anti-BSH mouse mAb and Cy3-conjugated mouse IgG were used as the primary and secondary antibody. Red fluorescence of Cy3 was used to show the distribution of BSH and blue fluorescence of hochest was used to indicate the position of the tumor. (A,D,G) Cy3-fluorescence images (10×). (C,F,I) Hochest-fluorescence images (10×). (B,E,H) Merging of the Cy3 and hochest signals. Bar = 200 μm.

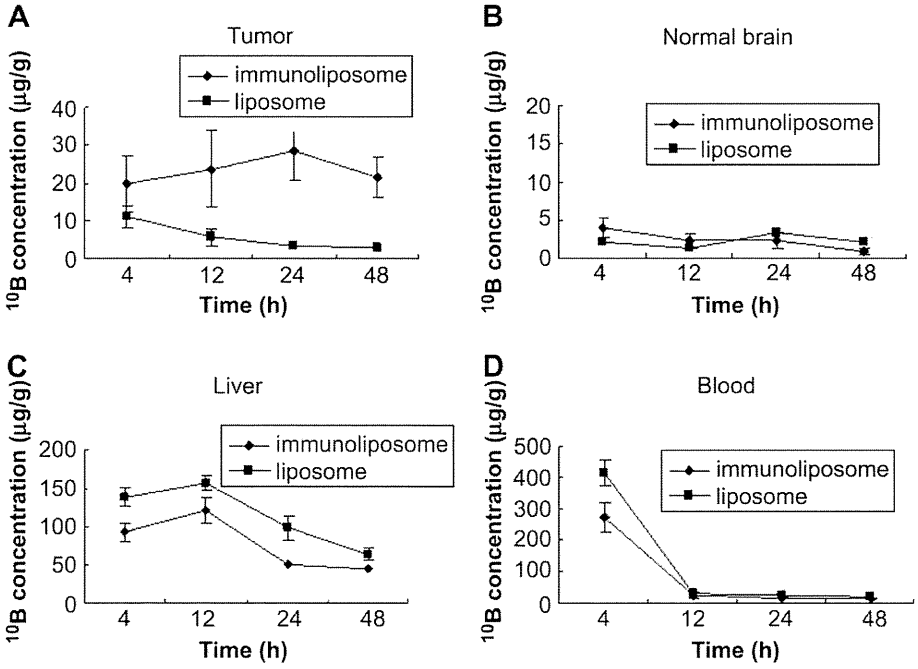

Fig. 8. Time course of ^{10}B's distribution *in vivo*. ^{10}B concentrations in tumor (A), normal brain (B), liver (C) and blood (D) were measured after 400 μL of immunoliposome or liposome was injected into tumor-bearing mice via a tail vein at a dose of 35 mg ^{10}B/kg.

fibers [38]. The tumor usually recurs after initial surgical resection. In BNCT, it is still difficult to deliver enough ^{10}B to the invading glioma cells in the brain. Our immunoliposomes may solve this problem. PEG-lipid and ZZ on the surface of the liposome provide steric stabilization and prolong circulation time. In solid tumors, the BBB is destroyed, and the abnormal tumor vessels are discontinuous, with pores varying from 100 to 780 nm [39,40]. At 4 h after an intravenous injection, the immunoliposome reached the tumor through the blood stream, and the anti-EGFR mAb effectively recognized the EGFR on the surface of tumor cells. The immunoliposomes had passed through the tumor vessel and penetrated tumor cells, as weak fluorescence could be seen in the blood vessel wall (Fig. 6A). At normal sites, we could see strong fluorescence on the surface of vessel walls and no fluorescence in normal tissues (Fig. 6E). This suggests that the immunoliposomes could not pass through the BBB in normal tissue.

To avoid possible toxic effects of DOGS-NTA-Ni, we are now exploring a new way to conjugate ZZ to the liposome surface. Our immunoliposomes can be used as a universal drug delivery system to deliver other anti-cancer drugs to tumor cells if we know the receptor or ligand on the surface of the tumor cells. In this study, ^{10}B delivery has been proved effective.

5. Conclusion

The results described above support the use of immunoliposomes to specifically deliver BSH to glioma cells. Recombinant ZZ-His (Fc-binding domain) was conjugated to liposomes containing 10 mol% DOGS-NTA-Ni and 1 mol% DSPE-PEG_{2000} to prepare immunoliposomes. This is the first time that an antibody-binding domain has been used to deliver ^{10}B in BNCT. ICP-AES and IHC indicated that ^{10}B was specifically delivered into EGFR-overexpresing glioma cells *in vitro* and *in vivo*. Thus, it appears that our system can be used for the specific delivery of other anti-cancer drugs.

Acknowledgements

We thank Dr. S. Kasaoka at Hiroshima International University for technical advice. This work was supported by a Grant-in-aid for Scientific Research from the Ministry of Education, Science, Sports and Culture of Japan and by a Grant-in-aid for Scientific Research from the Ministry of Health, Labour and Welfare of Japan.

Appendix

Figures with essential colour discrimination. Certain figures in this article, in particular parts of Figs. 2, 3, 4, 6 and 7, are difficult to interpret in black and white. The full colour images can be found in the online version, at doi:10.1016/j.biomaterials.2008.12.010.

Appendix. Supplementary material

Z-Dimensional scan of ^{10}B delivery by immunoliposomes in U87 ΔEGFR (100×). IHC was carried out as described in Fig. 4. Video was recorded at *Z*-sections from the bottom to top of cells every 2 μm. Supplementary data associated with this article can be found, in the online version, at doi:10.1016/j.biomaterials.2008.12.010.

References

[1] van Rij CM, Wilhelm AJ, Sauerwein WA, van Loenen AC. Boron neutron capture therapy for glioblastoma multiforme. Pharm World Sci 2005;27:92–5.
[2] Mehta SC, Lu DR. Targeted drug delivery for boron neutron capture therapy. Pharm Res 1996;13:344–51.
[3] Yanagië H, Ogata A, Sugiyama H, Eriguchi M, Takamoto S, Takahashi H. Application of drug delivery system to boron neutron capture therapy for cancer. Expert Opin Drug Deliv 2008;5:427–43.
[4] Barth RF, Coderre JA, Vicente MG, Blue TE. Boron neutron capture therapy of cancer: current status and future prospects. Clin Cancer Res 2005;11:3987–4002.
[5] Yokoyama K, Miyatake S, Kajimoto Y, Kawabata S, Doi A, Yoshida T, et al. Pharmacokinetic study of BSH and BPA in simultaneous use for BNCT. J Neurooncol 2006;78:227–32.
[6] Soloway AH, Hatanaka H, Davis MA. Penetration of brain and brain tumor. VII. Tumor-binding sulfhydryl boron compounds. J Med Chem 1967;10:714–7.
[7] Carlsson J, Kullberg EB, Capala J, Sjöberg S, Edwards K, Gedda L. Ligand liposomes and boron neutron capture therapy. J Neurooncol 2003;62:47–59.
[8] Hawthorne MF, Shelly K. Liposomes as drug vehicles for boron agents. J Neurooncol 1997;33:53–8.
[9] Sofou S, Sgouros G. Antibody-targeted liposomes in cancer therapy and imaging. Expert Opin Drug Deliv 2008;5:189–204.
[10] Pan XQ, Wang H, Lee RJ. Boron delivery to a murine lung carcinoma using folate receptor-targeted liposomes. Anticancer Res 2002;22:1629–33.
[11] Maruyama K, Ishida O, Kasaoka S, Takizawa T, Utoguchi N, Shinohara A, et al. Intracellular targeting of sodium mercaptoundecahydrododecaborate (BSH) to solid tumors by transferrin-PEG liposomes, for boron neutron-capture therapy (BNCT). J Control Release 2004;98:195–207.
[12] Bohl Kullberg E, Bergstrand N, Carlsson J, Edwards K, Johnsson M, Sjöberg S, et al. Development of EGF-conjugated liposomes for targeted delivery of boronated DNA binding agents. Bioconjug Chem 2002;13:737–43.
[13] Friedman HS, Bigner DD. Glioblastoma multiforme and the epidermal growth factor receptor. N Engl J Med 2005;353:1997–9.
[14] Yang W, Wu G, Barth RF, Swindall MR, Bandyopadhyaya AK, Tjarks W, et al. Molecular targeting and treatment of composite EGFR and EGFRvIII-positive gliomas using boronated monoclonal antibodies. Clin Cancer Res 2008;14:883–91.
[15] Schwechheimer K, Huang S, Cavenee WK. EGFR gene amplification-rearrangement in human glioblastomas. Int J Cancer 1995;62:145–8.
[16] Sauter G, Maeda T, Waldman FM, Davis RL, Feuerstein BG. Patterns of epidermal growth factor receptor amplification in malignant gliomas. Am J Pathol 1996;148:1047–53.
[17] Park JW, Hong K, Kirpotin DB, Papahadjopoulos D, Benz CC. Immunoliposomes for cancer treatment. Adv Pharmacol 1997;40:399–435.
[18] Ishida T, Iden DL, Allen TM. A combinatorial approach to producing sterically stabilized (Stealth) immunoliposomal drugs. FEBS Lett 1999;460:129–33.
[19] Iden DL, Allen TM. *In vitro* and *in vivo* comparison of immunoliposomes made by conventional coupling techniques with those made by a new post-insertion approach. Biochim Biophys Acta 2001;1513:207–16.
[20] Tsutsui Y, Tomizawa K, Nagita M, Michiue H, Nishiki T, Ohmori I, et al. Development of bionanocapsules targeting brain tumors. J Control Release 2007;122:159–64.
[21] Feng B, Zhao CH, Tanaka S, Imanaka H, Imamura K, Nakanishi K. TPR domain of Ser/Thr phosphatase of *Aspergillus oryzae* shows no auto-inhibitory effect on the dephosphorylation activity. Int J Biol Macromol 2007;41:281–5.
[22] Michiue H, Tomizawa K, Wei FY, Matsushita M, Lu YF, Ichikawa T, et al. The NH2 terminus of influenza virus hemagglutinin-2 subunit peptides enhances the antitumor potency of polyarginine-mediated p53 protein transduction. J Biol Chem 2005;280:8285–9.
[23] Tomizawa K, Iga N, Lu YF, Moriwaki A, Matsushita M, Li ST, et al. Oxytocin improves long-lasting spatial memory during motherhood through MAP kinase cascade. Nat Neurosci 2003;6:384–90.
[24] Doi A, Kawabata S, Iida K, Yokoyama K, Kajimoto Y, Kuroiwa T, et al. Tumor-specific targeting of sodium borocaptate (BSH) to malignant glioma by transferrin-PEG liposomes: a modality for boron neutron capture therapy. J Neurooncol 2008;87:287–94.
[25] Nielsen UB, Kirpotin DB, Pickering EM, Drummond DC, Marks JD. A novel assay for monitoring internalization of nanocarrier coupled antibodies. BMC Immunol 2006;7:24.
[26] Yokoyama K, Miyatake S, Kajiomoto Y, Kawabata S, Doi A, Yoshida T, et al. Analysis of boron distribution *in vivo* for BNCT using two different boron compounds by secondary ion mass spectroscopy. Radiat Res 2007;167:102–9.
[27] Mamot C, Drummond DC, Noble CO, Kallab V, Guo Z, Hong K, et al. Epidermal growth factor receptor-targeted immunoliposomes significantly enhance the efficacy of multiple anticancer drugs *in vivo*. Cancer Res 2005;24:11631–8.
[28] Mendelsohn J, Baselga J. Epidermal growth factor receptor targeting in cancer. Semin Oncol 2006;33:369–85.
[29] Pan X, Wu G, Yang W, Barth RF, Tjarks W, Lee RJ. Synthesis of cetuximab-immunoliposomes via a cholesterol-based membrane anchor for targeting of EGFR. Bioconjug Chem 2007;18:101–8.
[30] Chikh GG, Li WM, Schutze-Redelmeier MP, Meunier JC, Bally MB. Attaching histidine-tagged peptides and proteins to lipid-based carriers through use of metal-ion-chelating lipids. Biochim Biophys Acta 2002;1567:204–12.
[31] Lauer SA, Nolan JP. Development and characterization of Ni-NTA-bearing microspheres. Cytometry 2002;48:136–45.
[32] Patel JD, O'Carra R, Jones J, Woodward JG, Mumper RJ. Preparation and characterization of nickel nanoparticles for binding to His-tag proteins and antigens. Pharm Res 2007;24:343–52.
[33] van Broekhoven CL, Parish CR, Demangel C, Britton WJ, Altin JG. Targeting dendritic cells with antigen-containing liposomes: a highly effective

procedure for induction of antitumor immunity and for tumor immunotherapy. Cancer Res 2004;64:4357–65.
[34] Kamps JA, Scherphof GL. Receptor versus non-receptor mediated clearance of liposome. Adv Drug Deliv Rev 1998;32:81–97.
[35] Allen TM, Brandeis E, Hansen CB, Kao GY, Zalipsky S. A new strategy for attachment of antibodies to sterically stabilized liposome resulting in efficient targeting to cancer-cells. Biochim Biophys Acta 1995;1237: 99–108.
[36] Moks T, Abrahmsén L, Nilsson B, Hellman U, Sjöquist J, Uhlén M. Staphylococcal protein A consists of five IgG-binding domains. Eur J Biochem 1986;156:637–43.
[37] Hochuli E, Döbeli H, Schacher A. New metal chelate adsorbent selective for proteins and peptides containing neighbouring histidine residues. J Chromatogr 1987;411:177–84.
[38] Laerum OD, Bjerkvig R, Steinsvåg SK, de Ridder L. Invasiveness of primary brain tumors. Cancer Metastasis Rev 1984;3:223–36.
[39] Maruyama K, Takahashi N, Tagawa T, Nagaike K, Iwatsuru M. Immunoliposomes bearing polyethyleneglycol-coupled Fab′ fragment show prolonged circulation time and high extravasation into targeted solid tumors *in vivo*. FEBS Lett 1997;413:177–80.
[40] Siwak DR, Tari AM, Lopez-Berestein G. The potential of drug-carrying immunoliposomes as anticancer agents. Clin Cancer Res 2002;8:955–6.

Pseudoprogression in boron neutron capture therapy for malignant gliomas and meningiomas

Shin-Ichi Miyatake, Shinji Kawabata, Naosuke Nonoguchi, Kunio Yokoyama, Toshihiko Kuroiwa, Hideki Matsui, and Koji Ono

Department of Neurosurgery, Osaka Medical College, Osaka (S.-I.M., S.K., N.N., K.Y., T.K.); Department of Physiology, Okayama University, Graduate School of Medicine and Dentistry, Okayama (H.M.); Particle Radiation Oncology Research Center, Research Reactor Institute, Kyoto University, Kyoto (K.O.); Japan

Pseudoprogression has been recognized and widely accepted in the treatment of malignant gliomas, as transient increases in the volume of the enhanced area just after chemoradiotherapy, especially using temozolomide. We experienced a similar phenomenon in the treatment of malignant gliomas and meningiomas using boron neutron capture therapy (BNCT), a cell-selective form of particle radiation. Here, we introduce representative cases and analyze the pathogenesis. Fifty-two cases of malignant glioma and 13 cases of malignant meningioma who were treated by BNCT were reviewed retrospectively mainly via MR images. Eleven of 52 malignant gliomas and 3 of 13 malignant meningiomas showed transient increases of enhanced volume in MR images within 3 months after BNCT. Among these cases, five patients with glioma underwent surgery because of suspicion of relapse. In histology, most of the specimens showed necrosis with small amounts of residual tumor cells. Ki-67 labeling showed decreased positivity compared with previous samples from the individuals. Fluoride-labeled boronophenylalanine PET was applied in four and two cases of malignant gliomas and meningiomas, respectively, at the time of transient increase of lesions. These PET scans showed decreased lesion:normal brain ratios in all cases compared with scans obtained prior to BNCT. With or without surgery, all lesions were decreased or stable in size during observation. Transient increases in enhanced volume in malignant gliomas and meningiomas immediately after BNCT seemed to be pseudoprogression. This pathogenesis was considered as treatment-related intratumoral necrosis in the subacute phase after BNCT. *Neuro-Oncology 11, 430–436, 2009 (Posted to Neuro-Oncology [serial online], Doc. D08-00183, March 16, 2009. URL http://neuro-oncology.dukejournals.org; DOI: 10.1215/15228517-2008-107)*

Keywords: boron neutron capture therapy (BNCT), glioma, malignant meningioma, positron emission tomography (PET), pseudoprogression

With the advent of temozolomide (TMZ), concomitant chemoradiation and maintenance chemotherapy with TMZ has become the worldwide standard of care for malignant gliomas (MGs), especially glioblastoma multiforme (GBM).[1] With the spread of this chemoradiotherapy, pseudoprogression (psPD) has become a main topic in neurooncology, since it was reported by Chamberlain et al.[2] In their report, surgery confirmed necrosis without evidence of recurrent tumor in 7 (14%) of 51 patients with MG within 6 months after TMZ chemoradiotherapy. Because the definition of psPD has not been established universally, the incidence is difficult to estimate, but a high percentage has been reported, up to 21% for chemoradiotherapy using TMZ.[3] The main part of surgically resected samples showed necrosis, but the pathogenesis of psPD has not been fully elucidated.

Received July 13, 2008; accepted November 4, 2008.

Address correspondence to Shin-Ichi Miyatake, Department of Neurosurgery, Osaka Medical College, 2-7 Daigaku-machi, Takatsuki City, Osaka, 569-8686, Japan (neu070@poh.osaka-med.ac.jp).

We have applied a form of tumor-selective particle radiation, boron neutron capture therapy (BNCT), to MGs[4,5] and malignant meningiomas (MMs).[6,7] BNCT comprises a binary approach:[8] A boron-10 (^{10}B)-labeled compound is administered that delivers high concentrations of ^{10}B to the target tumor relative to the surrounding normal tissues. This is followed by irradiation with thermal neutrons. When neutrons collide into ^{10}B atoms, high–linear-energy-transfer (LET) alpha and ^{7}Li particles are released from the ^{10}B (n, alpha) ^{7}Li neutron capture reaction. The short range (5–9 μm) of these particles allows for relatively selective tumor killing with minimum damage to the adjacent normal brain tissue. These high-LET particles exert rapid and distinctive shrinkage of the mass not only in MG[4,5] but also in MM.[6,7] We noticed that in some cases of MG and in some cases of MM treated by BNCT, transient increases in enhanced volume in MR images[8] appeared just after BNCT.

Here we retrospectively review those cases that showed transient increases of enhanced volume in MR images within 3 months after BNCT. We analyzed these cases with histology and fluoride-labeled boronophenylalanine (F-BPA) PET data.

Materials and Methods

Patients

From 2002 to 2007, we used BNCT to treat 52 cases of MG (29 were newly diagnosed and 23 were recurrent cases) and 13 cases of recurrent MM. All the gadolinium (Gd)-enhanced MR images were retrospectively reviewed. The cases that showed transient increases of enhanced volume in MR images within 3 months after BNCT were picked up, and the characteristics were investigated as shown in Table 1. Case numbers were assigned sequentially for BNCT. Some cases underwent surgery for the suspicion of relapse, and for some cases tissue samples were analyzed with Ki-67 labeling.[9] Most cases underwent F-BPA-PET[4–7,10,11] before neutron irradiation, as described below, and some cases entered this study during the observation period when the enhanced area increased.

PET Scan

All F-BPA-PET scans were performed at Nishijin Hospital, Kyoto, Japan. BPA was originally synthesized as described previously,[12,13] and the protocol for PET measurements using a Headtome III tomograph (Shimadzu Co., Kyoto, Japan) has also been described elsewhere.[14,15] Briefly, regional BPA incorporation into tumors and contralateral brain tissue (as a nontumorous control area) was measured on PET images after an intravenous injection of F-BPA at a dose of 37–55.5 MBq (1–1.5 mCi) per 10 kg of body weight. PET images were collected continuously for a 60-min period, for a total of 15 periods. The lesions on the PET images were confirmed using contrast-enhanced MRI performed at levels equivalent to those used for the PET imaging studies. To obtain quantitative measurements using Amide software (SourceForge, Inc., Mountain View, CA, USA), oval regions of interest (ROIs) were placed on the tumors, including peak values in tumors of various sizes. At the corresponding level, the contralateral brain area was also chosen for ROI analysis. All of the macroscopically necrotic tumor areas observed on MR images were excluded when the ROIs were designated. We designated several ROIs from tumor-affected areas and adopted regions with the highest values as representative ROIs.

Table 1. Characteristics of cases that showed transient increases of enhanced volume in MR images within 3 months after BNCT

Case	Histology	New or Recurrent	RT Pre-BNCT	RT Post-BNCT	First PET L/N Ratio	Second PET L/N Ratio	Maximum BNCT (Gy-Eq)	Minimum BNCT (Gy-Eq)	Exploratory Surgery
Case 1	GBM	Recurrent	60 Gy	—	7	—	64.1	34.4	–
Case 4	GBM	New		SRS	—	—	50.6	23.8	+
Case 5	GBM	New		BNCT[a]	7.8	—	108.7	47.4	+
Case 10	GBM	Recurrent	80 Gy		2.8	—	48.3	27.2	+
Case 14	GBM	New		BNCT[b]	5.1	—	141	37.1	+
Case 15	AA	Recurrent	60 Gy		3.1	—	55.9	33.7	+
Case 35	GBM	New		30 Gy	—	—	90.6	61.4	–
Case 46	GBM	New		30 Gy	4.8	2	115	63	–
Case 48	GBM	Recurrent	60 Gy		3.3	1.7	50.5	49.2	–
Case 51	GBM	New		20 Gy	2.6	1.5	64	44.6	–
Case 57	AA	Recurrent	60 Gy		4.7	2.1	104.2	44.9	–
Case 33	MM	Recurrent	60 Gy + SRS		2.8	1.8	55.1	29.8	–
Case 50	MM	Recurrent	50 Gy		3.2	1.9	75.8	18.8	–
Case 56	MM	Recurrent	50 Gy		4.4	—	111.5	50.7	–

Abbreviations: BNCT, boron neutron capture therapy; RT, radiotherapy; L/N, lesion:normal brain; Gy-Eq, gray-equivalent; GBM, glioblastoma multiforme; SRS, stereotactic radiosurgery; AA, anaplastic astrocytoma; MM, malignant meningioma.

[a]BNCT was applied twice, because patient moved during the neutron irradiation during the first BNCT.

[b]BNCT was intentionally applied twice.

Clinical Regimen of BNCT

Candidates for BNCT routinely received F-BPA-PET to assess the distribution of boronophenylalanine (BPA).[10,11] The lesion:normal brain (L/N) ratio of BPA uptake can be estimated from this type of study, and dose planning was performed according to the L/N ratio, as described previously.[4,5]

The patients were administered 100 mg/kg sodium borocaptate for 1 h intravenously 12 h prior to neutron irradiation and 250–700 mg/kg BPA was administered for 1–6 h just prior to neutron irradiation. Amounts of BPA were decided by the disease and protocols as described previously.[4–6] The neutron irradiation time was determined not to exceed 15 Gy-Eq (gray-equivalents) to the normal brain by simulation. Here, Gy-Eq corresponds to the biologically equivalent x-ray dose that would have equivalent effects on tumors and on the normal brain.

Dose estimation of BNCT was done as follows. Blood was sampled every 2 h after sodium borocaptate administration until neutron irradiation was completed, to monitor the boron concentration in the blood. The boron concentration from sodium borocaptate in the blood during neutron irradiation was estimated from the measured ^{10}B concentration–time relationship. From previous BNCT experience, which was performed with craniotomy, we hypothesized that the boron concentrations in tumor and blood contributed from sodium borocaptate were equal just prior to neutron irradiation. We confirmed that BPA concentration in blood is equal to that in normal brain. Therefore, the boron concentrations from BPA in the tumor and normal brain were estimated from BPA concentration in blood by the L/N ratio of BPA-PET, as described above. Judging from these boron concentrations contributed from each boron compound, neutron fluence rate simulated by a dose-planning program, and the factors of relative biological effectiveness of neutron beam and each compound,[4] total doses to tumor and normal brain could be estimated, as in the following formula:[16]

$$\text{Equivalent dose (Gy-Eq)} = D_B \times CBE_B + D_N \times RBE_N + D_\gamma \times \text{hour},$$

where D_B is the boron dose (Gy) = $7.43 \times 10^{-14} \times$ boron concentration (μg ^{10}B/g) × thermal neutron fluence (Φ, calculated as the thermal neutron fluence rate [n/cm^2/s] × radiation time); D_N is the nitrogen dose (Gy) = $6.78 \times 10^{-14} \times$ nitrogen concentration (weight %) × Φ; and D_γ is the gamma-ray dose = 0.83 Gy/h.

Briefly, boron dose correlates to the ^{10}B concentration in the tissue and neutron fluence. Neutron fluence decays more in the deeper part of the tissue. Therefore, even in the same tumor, boron dose decreases in the deeper part compared with the superficial part of the tumor.

Results

Eleven of 52 cases of MG and 3 of 13 cases of MM showed transient increases of enhanced volume in MR images within 3 months after BNCT (Table 1). Among the 11 MG cases, five were recurrent and had been treated with fractionated x-ray treatment (XRT) prior to BNCT. The other six were newly diagnosed gliomas and were treated with two sessions of BNCT or with BNCT followed by fractionated XRT with 20–30 Gy. All MM cases listed in Table 1 were recurrent cases and had been treated with fractionated XRT with and without stereotactic radiosurgery.

Among the 11 cases of MG, five underwent surgery for suspicion of relapse when the mass increased in size after BNCT. The other six cases of MG and three cases of MM were followed up without additional surgery.

F-BPA-PET was applied in four and two cases of MGs and MMs, respectively, at the time of transient increase of lesions. Of these four MGs, two were newly diagnosed and two were recurrent cases. These PET scans showed decreased L/N ratios in all cases compared with scans obtained prior to BNCT (Table 1).

Representative Case Presentation: Case 5

Case 5 was a 70-year-old male with the manifestation of motor-dominant aphasia. He received surgery at first with the histological diagnosis of GBM. The tumor was partially removed. He was treated with BNCT twice with a 1-month interval. The enhanced mass on MR images shrank rapidly 5 weeks after the first BNCT (Fig. 1A-2); however, the enhanced lesion and perilesional edema became enlarged 2 months after initial BNCT (Fig. 1A-3). He received no chemotherapy. With this increase in lesion size, motor aphasia became slightly aggravated. The patient received recraniotomy 3 months after initial BNCT because tumor recurrence was suspected. Hematoxylin and eosin (H&E) staining and Ki-67 immunohistochemistry were applied to samples obtained at the first and second craniotomy (Fig. 2). H&E staining of the sample obtained at the second craniotomy showed necrosis in the main part, with ambiguously viable tissue. Ki-67 staining showed decreased positivity in the second surgical specimen compared with the first surgical specimen. Three months after the second craniotomy, the original lesion was stable in MR images, but tumor progression (TP) was recognized as cerebrospinal fluid (CSF) dissemination (Fig. 1A-4).

Representative Case Presentation: Case 35

Case 35 was a patient with newly diagnosed left temporal GBM. He received surgery with partial tumor removal (Fig. 1B-1) and was treated with BNCT followed by 20 Gy XRT without chemotherapy. This combination of radiotherapy resulted in drastic shrinkage of the mass within a month (Fig. 1B-2). However, 2 months after BNCT, motor aphasia was aggravated and MR images showed an increase of the enhanced area (Fig.

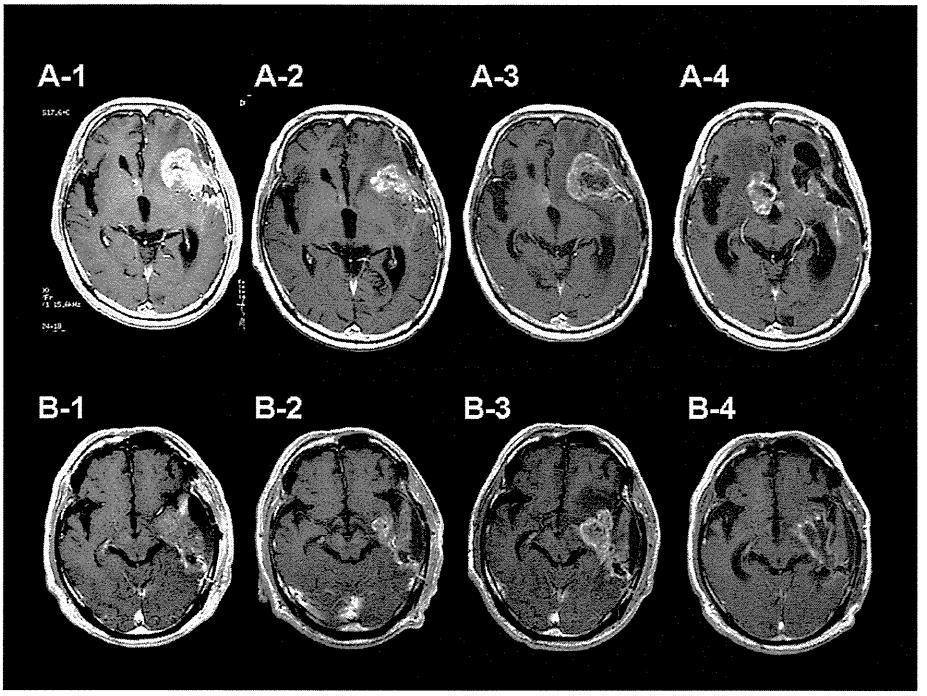

Fig. 1. Two representative cases of pseudoprogression of newly diagnosed glioblastoma multiforme treated by boron neutron capture therapy (BNCT). (A-1–A-4) Gadolinium (Gd)-enhanced MR images of case 5: prior to BNCT (A-1), 5 weeks after BNCT (A-2), 2 months after BNCT (A-3), and 6 months after BNCT and 3 months after second craniotomy (A-4). Case 5 was operated on 3 months after BNCT for the suspicion of tumor progression (judged from A-3). The operated lesion was stable for more than 3 months without chemotherapy. (B-1–B-4) Gd-enhanced MR images of case 35: prior to BNCT (B-1), 1 month after BNCT (B-2), 2 months after BNCT (B-3), and 7 months after BNCT (B-4).

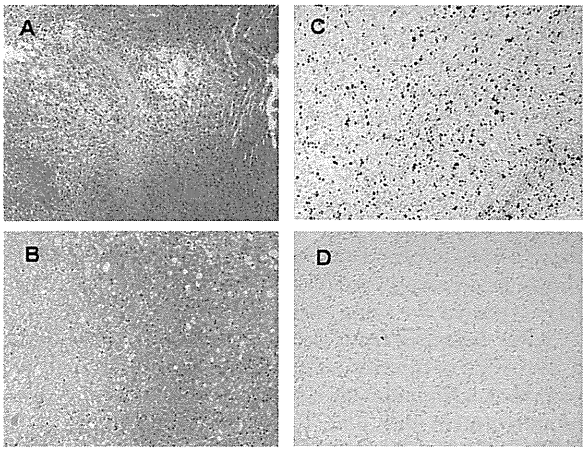

Fig. 2. Hematoxylin and eosin (H&E) and Ki-67 staining of specimens obtained from the first and second craniotomy of case 5. (A and B) H&E staining of the specimen of first craniotomy (A) and second craniotomy (3 months after boron neutron capture therapy [BNCT]; B). (C and D) Ki-67 staining of the specimen of the first craniotomy (C) and second craniotomy (3 months after BNCT; D). Original magnification, ×200 for A–D.

1B-3). The lesion was controlled well by steroids, and the enhanced area decreased in size on follow-up MR images (Fig. 1B-4). We lost this case due to uncontrollable hydrocephalus by CSF dissemination.

Representative Case Presentation: Cases 50 and 56

Both patients had recurrent MMs and had been treated with repetitive surgery and fractionated XRT with 50 Gy. Case 50 had rhabdoid meningioma. BNCT also showed shrinkage of the mass (Fig. 3A-2) with transient increase of enhanced volume (Fig. 3A-3). The enhanced mass gradually shrank, again without any treatment (Fig. 3A-4). Case 56 had anaplastic meningioma. In this case, BNCT did not show prominent reduction of mass size but showed decreased enhancement in tumor mass just after BNCT (Fig. 3B-2). However, the mass became voluminous 2.5 months after BNCT and spontaneously decreased again in size and in enhancement of the core of the mass, with decreased perilesional edema (Fig. 3B-4). In both cases, BNCT could well control the mass locally, but we lost these cases by uncontrollable, shunt-ineffective hydrocephalus due to CSF dissemination.

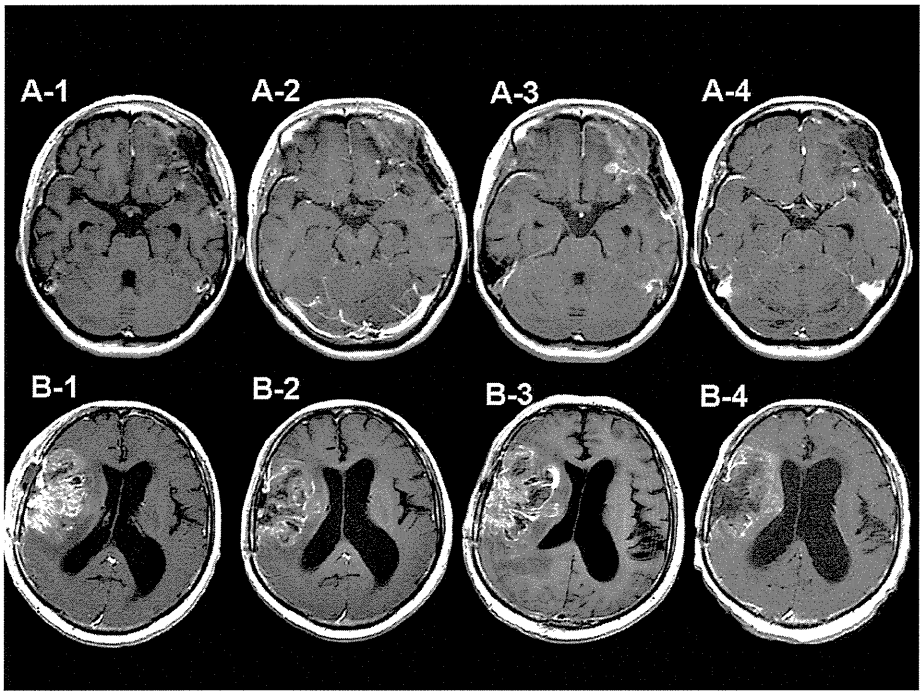

Fig. 3. Two representative cases of pseudoprogression of recurrent malignant meningiomas treated by boron neutron capture therapy (BNCT). (A-1–A-4) Gadolinium (Gd)-enhanced MR images of case 50: prior to BNCT (A-1), 48 h after BNCT (A-2) 1 month after BNCT (A-3), and 2 months after BNCT (A-4). (B-1–B-4) Gd-enhanced MR images of case 56: prior to BNCT (B-1), 1.5 months after BNCT (B-2), 2.5 months after BNCT (B-3), and 6 months after BNCT (B-4).

Discussion

psPD does not have a definitive definition. If we tentatively define psPD as a transient increase of enhanced volume in relatively early phases after some treatments without TP, a high incidence of psPD is reported.[3] psPD in MG has been recognized widely with the advent of TMZ treatment, and XRT alone has been reported to cause psPD.[17–20] However, combining some chemotherapeutic agents such as TMZ with XRT causes psPD with higher frequency and earlier compared with XRT alone.[2,3]

With BNCT, 11 of 52 MG and 3 of 13 MM cases experienced psPD, based on the above tentative definition. Six of 29 newly diagnosed MG cases and 5 of 23 recurrent MG cases showed psPD. We do not know the exact incidence of psPD with BNCT, because we could not review all MR images of all patients, and not all the patients received MRI at the same schedule in each hospital before being referred to our institute for BNCT. However, we do know that psPD occurred in these cases only by BNCT without chemotherapy, because we did not apply any chemotherapeutic agents until TP definitively occurred. In this article, we reviewed the cases that showed increased enhanced volume within 3 months after BNCT. In these cases, there was no true TP; however, we experienced two cases in whom true TP was proven by surgical specimen. They showed increased enhanced volume 4 months and 5 months after BNCT, respectively. We lost these two cases by local TP. Therefore, 3 months after BNCT seems to be an appropriate time period to review for psPD in BNCT.

The five cases of MG that received BNCT relatively early after diagnosis received surgery for suspicion of true TP. In these five cases, surgical specimens showed large necrotic areas with some viable cells with bizarre appearance, as shown in Fig. 2B. It is very difficult to determine whether these cells were derived from tumors and had proliferative activity based only on H&E staining.[21] Therefore, for case 5 we used Ki-67 staining, which showed decreased proliferative activity. Elsewhere, we have reported the same phenomenon in case 4.[5]

After learning from these earlier cases, we applied F-BPA-PET to discriminate psPD from true TP, as listed in Table 1. Originally, we developed F-BPA-PET for planning treatment with BNCT.[4–6,10,11] We then noticed that F-BPA-PET is useful to differentiate radiation necrosis (RN) and true TP, especially with repetitive analysis.[22] In our limited experience, pure RN always showed L/N ratios less than 1.9, and RN with small number of viable tumor cells showed L/N ratios less than 2.2.[22] Generally speaking, amino acid tracer has been used and is suitable for analyzing metabolism in malignant brain tumors[23,24] as well as for differentiating between RN and true TP,[24] because of low background activity compared with fluorodeoxyglucose-PET. We therefore applied F-BPA-PET and obtained reliable results, as shown here. As stated above, we almost always applied F-BPA-PET prior to

BNCT, so it was easy to compare the L/N ratio between the first PET obtained before BNCT and the second PET obtained when psPD, RN, or true TP was suspected.[22] In our BPA-PET series of recurrent GBM, all L/N ratios prior to BNCT were greater than 2.5, and L/N ratios of GBM at recurrence after BNCT were also greater than 2.5. Therefore, at least regarding GBM, when the tumor shows increase of enhancement in MRI within 3 months after BNCT, we may wait and see if the L/N ratio is less than 2.2.[22] In any case, early discrimination between psPD and true TP is important to apply potent alternative treatment for true TP patients without time delay.

The absorbed dose by BNCT, listed in Table 1, is applied only once. By BNCT we can deliver an enormous absorbed dose to tumor tissue. The range of maximum tumor dose by BNCT was 48.3–141 Gy-Eq, and the minimum dose range was 18.8–63.0 Gy-Eq (Table 1). These doses were applied at once. These values can be estimated approximately as 234.7–1,774.2 Gy and 45.1–383.3 Gy as given in daily doses of 2 Gy by fractionated XRT, with the assumption of α/β value of 10 Gy in the linear-quadratic model. We are not certain of the threshold of BNCT dose to cause psPD. The recurrent cases listed here received especially high doses overall, considering the addition of previous XRT, so psPD may frequently occur after BNCT in recurrent MG cases, because reirradiation is known as a risk factor for RN.[25,26] The latter half of the cases of newly diagnosed MG treated by BNCT in our protocol received fractionated XRT boosts with 20–30 Gy to decrease the possibility of recurrence.[16] Therefore, these high amounts of radiation might be a cause of marked psPD in BNCT cases. Because we did not apply any chemotherapy after BNCT until TP was confirmed by histology or PET, psPD described here may be caused only by radiation effects. Among the GBM patients treated with chemoradiation using TMZ, a high incidence of psPD was observed in methylated O^6-methylguanine-DNA methyltransferase (MGMT) promoter status, and those cases that exhibited psPD showed good prognosis compared with the cases of unmethylated MGMT promoter.[27] Taken together, intensive treatments may be the primary factor of psPD in MG, as Brandsma et al. reported.[28]

So far, we are not sure of the true mechanism of psPD. If psPD occurs by the same mechanism as the acute and subacute phase of radiation injury, psPD may be presumably caused by vasodilatation, disruption of the blood–brain barrier, and edema, due to endothelial cell damage.[29] Also, vascular endothelial growth factor (VEGF) may play an important role in psPD as it does in RN. By this speculation, anti-VEGF antibody may be applicable for symptomatic psPD.[30]

As stated above, more effective treatments may also result in higher incidences of psPD.[28] If this is true, high-LET and high relative-biological-effectiveness particle radiation, such as BNCT, may cause psPD frequently. Also, it is difficult to discriminate RN and psPD, especially with high-LET radiotherapy such as BNCT. We actually omitted one recurrent GBM case with possible psPD because it was difficult to discriminate the case from RN. We will probably observe the same phenomenon by these modalities. We would like to stress that psPD can occur not only with MG but also with MM by BNCT. Because all the incidences of psPD in our BNCT series occurred within the original tumor, psPD by BNCT can be defined as intratumoral treatment-related necrosis in the subacute phase after BNCT.

Acknowledgments

This work was partly supported by Grants-in-Aid for Scientific Research (B) (16390422 and 19390385) from the Ministry of Education, Culture Sports, Science, and Technology (MEXT) of Japan; a Grant-in-Aid for Scientific Research from the Ministry of Health, Labour, and Welfare of Japan to S.-I.M.; the Regional Science Promotion Program of the Japan Science and Technology Corporation; and the "Second-Term Comprehensive 10-Year Strategy for Cancer Control" of the Ministry of Health, Labour, and Welfare of Japan to S.-I.M. This work was also supported in part by the Takeda Science Foundation for Osaka Medical College; a Grant-in-Aid for Cancer Research (12217065) from MEXT to K.O.; and a Grant-in-Aid for Scientific Research for Young Researchers (B) (18791030) from the Ministry of Education, Science, and Culture of Japan to S.K.

References

1. Stupp R, Mason WP, van den Bent MJ, et al. Radiotherapy plus concomitant and adjuvant temozolomide for glioblastoma. *N Engl J Med.* 2005;352:987–996.
2. Chamberlain MC, Glantz MJ, Chalmers L, Van Horn A, Sloan AE. Early necrosis following concurrent Temodar and radiotherapy in patients with glioblastoma. *J Neurooncol.* 2007;82:81–83.
3. Taal W, Brandsma D, de Bruin HG, et al. Incidence of early pseudoprogression in a cohort of malignant glioma patients treated with chemoirradiation with temozolomide. *Cancer.* 2008;113(2):405–410.
4. Kawabata S, Miyatake S, Kajimoto Y, et al. The early successful treatment of glioblastoma patients with modified boron neutron capture therapy. Report of two cases. *J Neurooncol.* 2003;65:159–165.
5. Miyatake S, Kawabata S, Kajimoto Y, et al. Modified boron neutron capture therapy for malignant gliomas performed using epithermal neutron and two boron compounds with different accumulation mechanisms: An efficacy study based on findings on neuroimages. *J Neurosurg.* 2005;103:1000–1009.
6. Miyatake S, Tamura Y, Kawabata S, Iida K, Kuroiwa T, Ono K. Boron neutron capture therapy for malignant tumors related to meningiomas. *Neurosurgery.* 2007;61:82–91.
7. Tamura Y, Miyatake S, Nonoguchi N, et al. Boron neutron capture therapy for recurrent malignant meningioma. Case report. *J Neurosurg.* 2006;105:898–903.
8. Coderre JA, Chanana AD, Joel DD, et al. Biodistribution of boronophenylalanine in patients with glioblastoma multiforme: Boron concentration correlates with tumor cellularity. *Radiat Res.* 1998;149:163–170.
9. Gerdes J, Lemke H, Baisch H, Wacker HH, Schwab U, Stein H. Cell cycle analysis of a cell proliferation-associated human nuclear antigen defined by the monoclonal antibody Ki-67. *J Immunol.* 1984;133:1710–1715.
10. Imahori Y, Ueda S, Ohmori Y, et al. Positron emission tomography-based boron neutron capture therapy using boronophenylalanine for high-grade gliomas: Part I. *Clin Cancer Res.* 1998;4:1825–1832.
11. Imahori Y, Ueda S, Ohmori Y, et al. Positron emission tomography-based boron neutron capture therapy using boronophenylalanine for high-grade gliomas: Part II. *Clin Cancer Res.* 1998;4:1833–1841.
12. Ishiwata K, Ido T, Mejia AA, Ichihashi M, Mishima Y. Synthesis and radiation dosimetry of 4-borono-2-[^{18}F]fluoro-D,L-phenylalanine: A target compound for PET and boron neutron capture therapy. *Int J Rad Appl Instrum A.* 1991;42:325–328.
13. Mishima Y, Imahori Y, Honda C, Hiratsuka J, Ueda S, Ido T. In vivo diagnosis of human malignant melanoma with positron emission tomography using specific melanoma-seeking 18F-DOPA analogue. *J Neurooncol.* 1997;33:163–169.
14. Imahori Y, Ueda S, Ohmori Y, et al. Fluorine-18-labeled fluoroboronophenylalanine PET in patients with glioma. *J Nucl Med.* 1998;39:325–333.
15. Takahashi Y, Imahori Y, Mineura K. Prognostic and therapeutic indicator of fluoroboronophenylalanine positron emission tomography in patients with gliomas. *Clin Cancer Res.* 2003;9:5888–5895.
16. Kawabata S, Miyatake S, Kuroiwa T, et al. Boron neutron capture therapy for newly diagnosed glioblastoma. *J Rad Res.* In press.
17. de Wit MC, de Bruin HG, Eijkenboom W, Sillevis Smitt PA, van den Bent MJ. Immediate post-radiotherapy changes in malignant glioma can mimic tumor progression. *Neurology.* 2004;63:535–537.
18. Fiegler W, Langer M, Scheer M, Kazner E. Reversible computed tomographic changes following brain tumor irradiation induced by the "early-delayed reaction" after radiation [in German]. *Der Radiologe.* 1986;26:206–209.
19. Griebel M, Friedman HS, Halperin EC, et al. Reversible neurotoxicity following hyperfractionated radiation therapy of brain stem glioma. *Medical Pediatr Oncol.* 1991;19:182–186.
20. Watne K, Hager B, Heier M, Hirschberg H. Reversible oedema and necrosis after irradiation of the brain. Diagnostic procedures and clinical manifestations. *Acta Oncol.* 1990;29:891–895.
21. Perry A, Schmidt RE. Cancer therapy-associated CNS neuropathology: An update and review of the literature. *Acta Neuropathol.* 2006;111:197–212.
22. Miyashita M, Miyatake S, Imahori Y, et al. Evaluation of fluoride-labeled boronophenylalanine-PET imaging for the study of radiation effects in patients with glioblastomas. *J Neurooncol.* 2008;89:239–246.
23. Ceyssens S, Van Laere K, de Groot T, Goffin J, Bormans G, Mortelmans L. [^{11}C]methionine PET, histopathology, and survival in primary brain tumors and recurrence. *AJNR Am J Neuroradiol.* 2006;27:1432–1437.
24. Tsuyuguchi N, Takami T, Sunada I, et al. Methionine positron emission tomography for differentiation of recurrent brain tumor and radiation necrosis after stereotactic radiosurgery—in malignant glioma. *Ann Nucl Med.* 2004;18:291–296.
25. Bauman GS, Sneed PK, Wara WM, et al. Reirradiation of primary CNS tumors. *Int J Radiat Oncol Biol Phys.* 1996;36:433–441.
26. Mayer R, Sminia P. Reirradiation tolerance of the human brain. *Int J Radiat Oncol Biol Phys.* 2008;70:1350–1360.
27. Brandes AA, Franceschi E, Tosoni A, et al. MGMT promoter methylation status can predict the incidence and outcome of pseudoprogression after concomitant radiochemotherapy in newly diagnosed glioblastoma patients. *J Clin Oncol.* 2008;26:2192–2197.
28. Brandsma D, Stalpers L, Taal W, Sminia P, van den Bent MJ. Clinical features, mechanisms, and management of pseudoprogression in malignant gliomas. *Lancet Oncol.* 2008;9:453–461.
29. Wong CS, Van der Kogel AJ. Mechanisms of radiation injury to the central nervous system: Implications for neuroprotection. *Mol Interv.* 2004;4:273–284.
30. Gonzalez J, Kumar AJ, Conrad CA, Levin VA. Effect of bevacizumab on radiation necrosis of the brain. *Int J Radiat Oncol Biol Phys.* 2007;67:323–326.

J Neurooncol (2009) 91:199–206
DOI 10.1007/s11060-008-9699-x

CLINICAL STUDY - PATIENT STUDY

Survival benefit of Boron neutron capture therapy for recurrent malignant gliomas

Shin-Ichi Miyatake · Shinji Kawabata · Kunio Yokoyama · Toshihiko Kuroiwa · Hiroyuki Michiue · Yoshinori Sakurai · Hiroaki Kumada · Minoru Suzuki · Akira Maruhashi · Mitsunori Kirihata · Koji Ono

Received: 18 June 2008 / Accepted: 8 September 2008 / Published online: 24 September 2008

Abstract We have applied boron neutron capture therapy (BNCT) to malignant brain tumors. Here we evaluated the survival benefit of BNCT for recurrent malignant glioma (MG). Since 2002, we have treated 22 cases of recurrent MG with BNCT. Survival time was analyzed with special reference to recursive partitioning analysis (RPA) classification, by Carson et al. (J Clin Oncol 25:2601–2606, 2007). Median survival times (MSTs) after BNCT for all patients and for glioblastoma as on-study histology at recurrence was 10.8 months ($n = 22$; 95% CI, 7.3–12.8 months) and 9.6 months ($n = 19$; 95% CI, 6.9–11.4 months), respectively. In our study, MST for the high-risk RPA classes was 9.1 months ($n = 11$; 95% CI, 4.4–11.0 months). By contrast, the original journal data showed that the MST of the same RPA classes was 4.4 months ($n = 129$; 95% CI, 3.6–5.4 months). BNCT showed a survival benefit for recurrent MG, especially in the high-risk group.

Keywords BNCT · BPA–PET · GBM · MG · RPA

Electronic supplementary material The online version of this article (doi:10.1007/s11060-008-9699-x) contains supplementary material, which is available to authorized users.

S.-I. Miyatake (✉) · S. Kawabata · K. Yokoyama · T. Kuroiwa
Department of Neurosurgery, Osaka Medical College, 2-7 Daigaku Machi, Takatsuki, Osaka 569–8686, Japan
e-mail: neu070@poh.osaka-med.ac.jp

S.-I. Miyatake
Cancer Intelligence Care System, Inc., Tokyo, Japan

H. Michiue
Department of Neurosurgery, Okayama University, Okayama, Japan

Y. Sakurai · M. Suzuki · A. Maruhashi · K. Ono
Particle Radiation Oncology Research Center, Research Reactor Institute, Kyoto University, Kumatori, Japan

H. Kumada
Department of Research Reactor and Tandem Accelerator, Nuclear Science Institute, Japan Atomic Energy Agency, Tokai, Japan

M. Kirihata
Department of Agriculture, Osaka Prefectural University, Sakai, Japan

Introduction

We have applied a form of tumor-selective particle radiation, boron neutron capture therapy (BNCT), for malignant gliomas (MGs) [1, 2] and malignant meningiomas [3, 4]. BNCT comprises a binary approach [5]: a boron-10 (^{10}B)-labeled compound is administered that delivers high concentrations of ^{10}B to the target tumor relative to the surrounding normal tissues. This is followed by irradiation with thermal neutrons. When neutrons collide into ^{10}B atoms, high linear-energy-transfer (LET) alpha and ^{7}Li particles are released from the ^{10}B (n, alpha) ^{7}Li neutron capture reaction. The short range (5–9 micrometers) of these particles allows for relatively selective tumor killing without significant damage to the adjacent normal brain tissue.

The prognosis of recurrent MGs, especially glioblastoma multiforme (GBM) is poor [6]. We reported the effectiveness of BNCT on neuroimages for MGs [1, 2], and recently reported the survival benefit of BNCT for newly diagnosed MGs [7]. Unfortunately, the standard treatment for recurrent MG has not yet been established. Therefore, evaluation of the survival benefit of BNCT for recurrent MGs is difficult. Also with limited case numbers like this study, it is difficult to elucidate some objective assessments